Electronic structure of the Ca_3Co_4O_9 compound from ab initio local interactions

Julien Soret, Marie-Bernadette Lepetit

Electronic structure of the $Ca_3Co_4O_9$ compound from ab initio local interactions

Julien Soret[1] and Marie-Bernadette Lepetit[1]

[1] *CRISMAT, ENSICAEN-CNRS UMR6508, 6 bd. Maréchal Juin, 14050 Caen, FRANCE*

(Dated: June 14, 2011)

We used fully correlated ab initio calculations to determine the effective parameters of Hubbard and t − J models for the thermoelectric misfit compound $Ca_3Co_4O_9$. As for the Na_xCoO_2 family the Fermi level orbitals are the a_{1g} orbitals of the cobalt atoms ; the e'_g being always lower in energy by more than 240 meV. The electron correlation is found very large $U/t \sim 26$ as well as the parameters fluctuations as a function of the structural modulation. The main consequences are a partial a_{1g} electrons localization and a fluctuation of the in-plane magnetic exchange from AFM to FM. The behavior of the Seebeck coefficient as a function of temperature is discussed in view of the ab initio results, as well as the 496 K phase transition.

I. INTRODUCTION

First studied for their ionic conduction properties[1], the layered cobalt oxides have been, in the last years, the object of a regained attention, due to the discovery of peculiar transport and magnetic properties. One can cite, for instance, the superconducting state of the $Na_{0.35}CoO_2 - 1.3H_2O$,[2] the large thermoelectric power (TEP) in the $Na_{0.7}CoO_2$,[3] or the rich phases diagram of the Na_xCoO_2 family.[4] In terms of applications the large thermoelectric power (TEP) found in some materials of this family is certainly the most interesting property. Indeed, in addition to Seebeck coefficients larger than $100\mu V/K$ at room temperature, these systems present the atypical association of a low resistivity and a low thermal conductivity. It results a large figure of merit $ZT = S^2T/\rho\kappa$ at room temperature[5,6] (where Z is the factor of merit, S the Seebeck coefficient, T the temperature, ρ the electrical resistivity, κ the thermal conductivity).

The motivation was at the origin of the search for new compounds, based on the same CoO_2 layers (known to be responsible for the electronic and magnetic properties), but with better chemical stability than the Na_xCoO_2 ones. Indeed, in air, these systems can both easily accept water or other small molecules in between the CoO_2 layers and loose part of their sodium content, both processes affecting the desired properties. The main idea was to replace the alkaline layer by a more complex oxide one. Many systems were thus synthesized such as $Tl_\alpha[(Sr,Ca)_{1-\beta}]_{1+x}CoO_2$,[7] $Bi_\alpha[A_{0.75}Bi_{0.25}O]_{3+3x/2}CoO_2$ (A = Ca, Sr)[8], $Sr_2O_2CoO_2$,[9] etc.

Among these layered cobalt oxides, the so-called $Ca_3Co_4O_9$[10] ($[Ca_2CoO_3]_{0.62}[CoO_2]$) occupies a special place. Indeed, this chemically "simple" system has been used as the reference system for the study of the thermoelectric properties in CoO_2-based compounds. In addition to its interesting thermoelectric properties the $Ca_3Co_4O_9$ present puzzling magnetic transitions[11] with the inset of an incommensurate spin density wave (IC-SDW) at low temperature, an often called "ferrimagnetic" transition around 19 K and a transition interpreted as a cobalt spin state transition around 380 K. The long-range IC-SDW sets in place at 27 K however from 100 K a short range IC-SDW order is observed by muon relaxation[11].

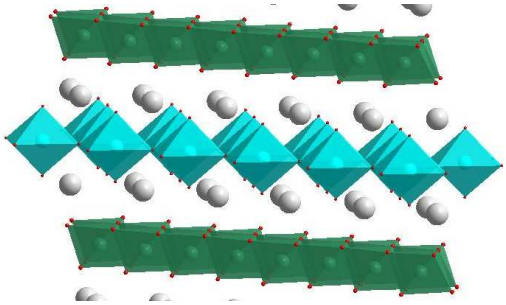

Figure 1. (Color online) Structural representation of the $Ca_3Co_4O_9$ compound. Green : CoO_2 layers of edge-sharing octahedra, blue : cobalt octahedra in the rock-salt layers and light gray : calcium ions.

The $Ca_3Co_4O_9$ system is built from the alternation of CdI_2-type CoO_2 layers and $CoCa_2O_3$ rock-salt-type layers[12] (see fig. 1). These layers are stacked along the $\vec{c}$-axis and present incommensurate lattice parameters along the $\vec{b}$ direction. The CoO_2 layers are built from edge-sharing cobalt octahedra presenting a compression along the $\vec{c}$ crystallographic direction (the octahedra (111) direction). The rock-salt layers are three-fold layers built from two Ca-O planes sandwiching a Co-O plane, or equivalently built from a layer of corner-sharing cobalt octahedra, as in a perovskite with the calcium atoms located at A sites. The incommensurability between the $\vec{b}$ lattice parameters of the two subsystems induces, in each layer, a structural modulation presenting the periodicity of the other subsystem. One of the important consequences is a distortion of the coordination sphere of each cobalt atom in the CoO_2 layers (different Co-Co distances, different Co-O distances and Co-O-Co angles). Indeed, the CoO_2 subsystem has been shown to be responsible for the low energy properties of the compound (transport, TEP, magnetism, etc.), since it supports the Fermi level electrons[6,10] while the $CoCa_2O_3$ subsystem was proved to be gapped. In addition, in the related

Na_xCoO_2 family the Fermi level properties were proved to be strongly dependant both on the doping[4] and on the local structural parameters[13].

The purpose of the present work will thus be to study the effect of the incommensurate modulations on the low energy degrees of freedom of the $Ca_3Co_4O_9$ system. At this point one should notice that, unfortunately, density functional (DFT) electronic structure calculations fail to properly describe the electronic structure of the CoO_2-based systems. Indeed, LDA as well as LDA+U calculations[14] exhibit a conducting $CoCa_2O_3$ subsystem dominating the density of states at the Fermi level. DFT is known to illy treat strong correlation effects, however, in many strongly correlated systems, it is nevertheless able to yield reasonable Fermi surfaces and the correct magnetic ground state. In the CoO_2-based systems, this is not the case. In the Na_xCoO_2 compounds DFT calculations yield a ferromagnetic ground state[15] while experimentally antiferromagnetic[16] and incorrect Fermi surfaces[17]. We will thus need to rely on alternating approaches, such as embedded cluster quantum chemical methods, explicitely treating the strong correlation at the Fermi level. Such methods also present the advantages to be able to treat the misfit character of the system. For this purpose we will use the same ab initio method that gave accurate and reliable results on the evaluation of such local effective parameters in other strongly correlated systems, that is the embedded fragment CAS+DDCI method[18]. This method yielded very good results in systems such as the copper or vanadium oxides[19], the Na_xCoO_2[13,20], etc., in periodic systems as well as misfit ones[21].

The modulated structures will be taken from reference[12]. We will compute the magnetic effective exchange between two nearest neighbors (NN) cobalt ions, the effective transfer, the correlation strength and the on-site parameters variations that could be responsible for electron localization.

II. METHOD AND COMPUTATIONAL DETAILS

The embedded fragment CAS+DDCI method is a spectroscopy method specifically designed to accurately treat the strongly correlated character of a set of orbitals (designed as active or magnetic orbitals), as well as the screening effects on all processes on this set of magnetic orbitals. Such a calculation implies large diagonalizations and can only be done on a formally finite system.

The embedded fragments are thus composed of a quantum part, treated within the CAS+DDCI quantum chemical method, and an embedding that reproduces the main effects of the rest of the crystal on the quantum part. The quantum part should include the cobalt ions involved in the sought interaction and their first coordination shell. Such a choice insures a proper treatment of the correlation effect on the cobalt $3d$ shell as well as the screening effects on the cobalt $3d$ electrons[18].

The main effects of the rest of the crystal on the quantum part are double. First, there is the short range exclusion of the quantum electrons from the space occupied by the electrons of the rest of the crystal. This effect is modeled using total ions pseudo-potentials[22] (TIPs) that represent the electronic structure of the first shells of atoms surrounding the quantum part. The second important effect is the Madelung potential. For this purpose, we used a set of renormalized charges. As far as the two periodic directions are concerned, we used the real space method developed by A. Gellé *et al.*[23] that reproduces the Madelung potential with an exponential convergence. For the incommensurate direction, we used the same method as in reference 21, imposing the nullity of both charge and dipole moment.

The question is now *"what formal charges should we use for the different atoms ?"*. The calcium and oxygen atoms will be taken as Ca^{2+} and O^{2-} ions. The question of the cobalt valence is a bit more difficult. Indeed, there is no reason for the cobalts to present the same valency in the two subsystems. Two arguments can help us in finding a reasonable evaluation of the charge transfer between the two layers. The first argument is a simple comparison between the average first neighbor cobalt–oxygen distances in the CoO_2 layers for $Ca_3Co_4O_9$ and for the Na_xCoO_2 family. With an average Co–O distance of 1.904Å the cobalt valence could be estimated from figure 5 of reference 24 to be similar to the $Na_{2/3}CoO_2$ system, that is about $Co^{3.33+}$ in the CoO_2 layer, and thus $Co^{3.05+}$ in the rock-salt layer. The second argument comes from a recent evaluation of the cobalt valency using atomic-column resolved energy-loss spectroscopy (EELS)[25]. Indeed Klie *et al* found a single valency of Co^{3+} in the rock-salt layers and a mixed valency in the CoO_2 layers. We thus used a Co^{3+} formal charge for the rock-salt subsystem and, insuring electro-neutrality, a $Co^{3.38}$ formal charge for the CoO_2 subsystem.

In the quantum calculations, the core electrons where treated using effective core potentials[26], while the valence and semi-valence electrons where treated using the associated Gaussian atomic basis set[26].

III. RESULTS : THE COBALT $3d$ ORBITALS

In the CoO_2 subsystem of the $Ca_3Co_4O_9$ compound, the cobalt ions are in a mixed valence state Co^{3+} ($3d^6$) and Co^{4+} ($3d^5$). It is sometimes written in the literature[10,27] that the Co^{3+} ions are in a low spin state while the Co^{4+} ion are in a high spin state. This assumption is in contradiction with what was found for the Na_xCoO_2 family where both cobalt ions are in a low spin state — Co^{3+} : $t_{2g}^6e_g^0$ and Co^{4+} : $t_{2g}^5e_g^0$. Since these $3d$ orbitals are responsible for the physical properties, it is of prime importance to first understand the cobalt $3d$ orbital splitting and spin states.

We thus computed the different spin states of a CoO_6

embedded fragment (Co^{3+} as well as Co^{4+} ionic states) for all crystallographically independent cobalt sites in the periodic directions, and a representative set of them in the misfit direction. We found that in all cases both the Co^{3+} and Co^{4+} ions are in a low spin state. Indeed, even for the Co^{4+} valence state the higher spin states are at least at 700 meV (~ 8000 K) above the low spin state.

As in the Na_xCoO_2 family, the CoO_6 octahedra are compressed along the $\vec{c}$ axis. One thus expects a splitting of the regular octahedron t_{2g} orbitals into a doublet e'_g and a singlet a_{1g}. The energetic order between these orbitals is crucial since it determines the nature of the magnetic orbitals of the Co^{4+} ions. A simple crystal field evaluation yields the e'_g orbitals at the Fermi level. However, it was shown that due to the O_h to S_6 symmetry reduction, the e'_g orbitals can and do hybridize with the high energy e_g ones. It results an energetic stabilization of the e'_g orbitals compared to the a_{1g} one and thus a non degenerated atomic ground state for the Co^{4+} ions[28] : $(e'_g)^4 a_{1g}$. In the present system the misfit character of the two subsystems tells us that further symmetry breaking occurs and that all cobalt $3d$ orbitals are non degenerated.

Figure 2 displays the $\varepsilon_{a_{1g}} - \varepsilon_{e'_g}$ orbital energy splitting as a function of the fourth crystallographic dimension parameter ($\tau = mod(n\, b_{CoO_2}/b_{RS}, 1)$, $n \in \mathbb{N}$ refers to the CoO_2 subsystem cells in the $\vec{b}$ direction — see figure 3 — b_{CoO_2} and b_{RS} are the lattice parameters of the two subsystems in the incommensurate direction) associated with the incommensurate modulations of the CoO_2 layers. Let us recall that this structural modulation takes place along the $\vec{b}$ direction. These effective orbital splittings where obtained as the energy difference of fully correlated ${e'_g}^4 {a_{1g}}^1$ and ${e'_g}^3 {a_{1g}}^2$ states of the CoO_6 embedded fragments. Indeed, these excitations energies can be associated with the effective orbital splitting of a 3-bands Hubbard model. One sees immediately that whatever the Co site, the a_{1g} orbital is always of higher energy than the e'_g ones ; that is the hole is always located in the a_{1g} orbital. The excitation energy for having a hole located in a e'_g orbital is always larger than 240 meV $\simeq 2800$ K. The average $\varepsilon_{a_{1g}} - \varepsilon_{e'_g}$ splitting is 261 meV, while the difference between the two e'_g orbitals ranges between 13 meV to 42 meV. Finally one should notice that the variations of the $\varepsilon_{a_{1g}} - \varepsilon_{e'_g}$ splitting as a function of the different crystallographic sites remains small ($< \pm 10$ meV).

As mentioned above the relative position of the a_{1g} and e'_g orbitals are related to the e'_g–e_g hybridization. As expected from the weak modulation of the orbital energy splitting, this hybridization remains stable, close for all sites to its average value of 10 degrees. This value is very comparable to the values found on different Na_xCoO_2 systems[13].

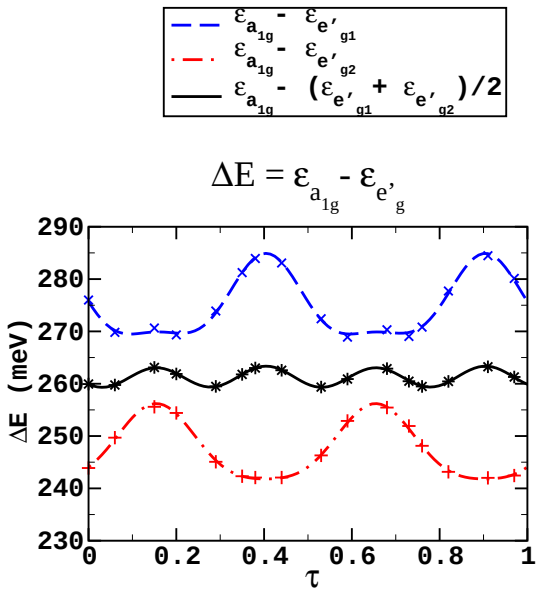

Figure 2. (Color online) $3d$ cobalt orbital energy splittings : $\varepsilon_{a_{1g}} - \varepsilon_{e'_g}$, as a function of the incommensurate modulation parameter τ. Blue curve with crosses : $\varepsilon_{a_{1g}} - \varepsilon_{e'_{g1}}$ splitting, red curve with plus signs : $\varepsilon_{a_{1g}} - \varepsilon_{e'_{g2}}$ splitting, black curve with stars : average $\varepsilon_{a_{1g}} - \varepsilon_{e'_g}$ splitting.

IV. RESULTS : a_{1g}-BASED ONE BAND MODELS

The previous section clearly told us that the a_{1g}–e'_g orbital splitting is large enough (2800 K) to justify a on-band model for our system. In this section we will thus extract from our calculations both the effective exchange integrals and the parameters of an extended Hubbard model from our ab-initio calculations.

The NN effective exchange can be obtained as the energy difference between the singlet and triplet states of the Co_2O_{10} embedded fragments. The extended Hubbard model parameters necessitate in addition the states wave functions information. Indeed, the parameters are determined so that the model reproduce both the singlet–triplet excitation energy and relative weight of the dominant configurations in the states wave functions. One should however notice that not all the parameters of the extended Hubbard model can be independently determined for the data. Indeed, only the NN hopping integral : t, the difference between the average on-site repulsion and the NN repulsion : $\bar{U} - V = (U_1 + U_2)/2 - V_{12}$ and the difference between the orbital energies and the on-site repulsions : $\delta\varepsilon_{a1g} - \delta U$ can be independently determined.

In this non-periodic system, the models parameters were determined for a representative set (sixteen dimers were computed) of incommensurate distortions values, then fitted as a function of the incommensurate dimension parameter τ.

One can define two types of non equivalent nearest

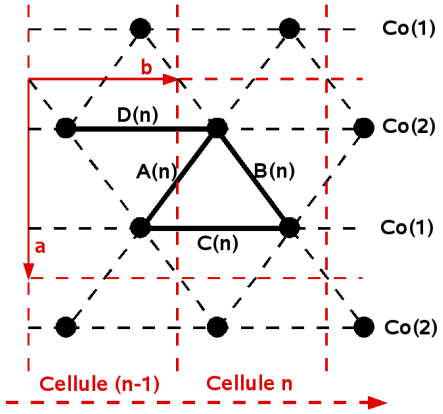

Figure 3. (Color online) Schematic representation of the different dimers.

neighbor dimers that propagate along the incommensurate $\vec{b}$ direction (see figure 3); the A dimers ($\vec{a} - \vec{b}$ direction) and the C dimers ($\vec{b}$ direction). Indeed, the B and D dimers can be deduced from the preceeding ones, through the expressions:

$$\tau_A \rightarrow \tau_B = 0.5\frac{b_{CoO_2}}{b_{RS}} - \tau_A \quad (1)$$

$$\tau_C \rightarrow \tau_D = -\tau_C \quad (2)$$

In the following discussions, we will refer to "$\vec{b}$ direction dimers" for the C and D dimers and to "$\vec{a} \pm \vec{b}$ directions dimers" for the A and B ones.

A. Effective exchange and hopping

Figure 4(a) reports the variations of the effective exchange integral J and figure 4(b) of the effective hopping integral t, as a function of the fourth crystallographic dimension parameter τ. Table I reports the parameters for the fit of the computed values according to the formula

$$J(\tau) = J_0 + J_1 \cos(2\pi[\tau + \varphi]) + J_2 \cos(4\pi[\tau + \varphi])$$
$$t(\tau) = t_0 + t_1 \cos(2\pi[\tau + \xi]) + t_2 \cos(4\pi[\tau + \xi]) \quad (3)$$

Dimer	J_0	J_1	J_2	φ	t_0	t_1	t_2	ξ
A	2.56	-6.38	1.36	0.00	-135.81	-38.15	12.65	0.00
C	-1.54	-0.02	3.49	0.60	-146.82	0.11	27.85	0.10

Table I. Parameters for effective exchange J and effective transfer t fits as a function of the incommensurate dimension parameter τ. The fitted values are associated with equations 3.

Let us notice the following points.

- The NN exchange J may be either antiferromagnetic (AFM) or ferromagnetic (FM) (resp. negative and positive) according to the specific dimer.

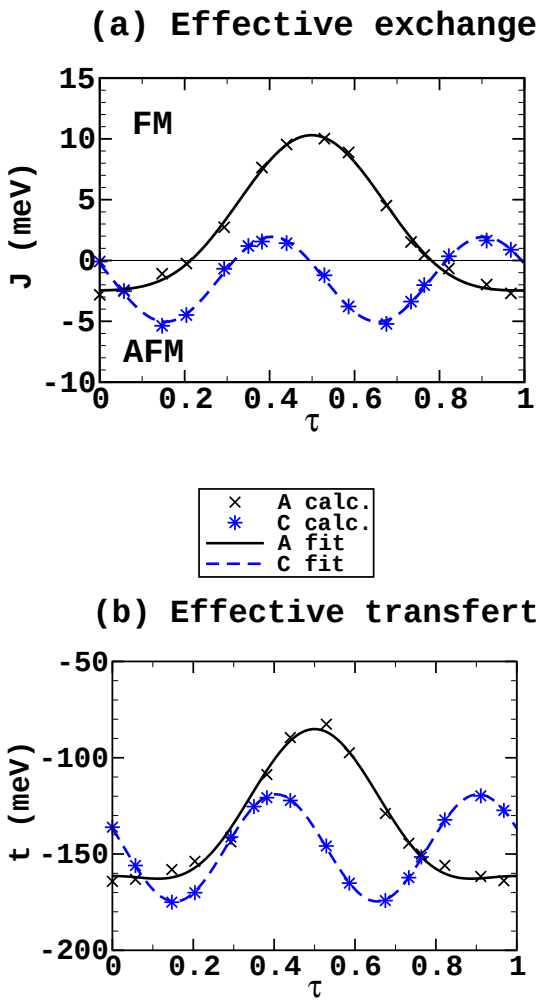

Figure 4. (Color online) (a) Effective exchange, J, and (b) effective transfer, t, as a function of the fourth crystallographic dimension parameter τ. Symbols represent the computed values, lines the fits.

- The NN exchange and hopping are strongly modulated for all dimer types. These modulations are essentially related to the Co-O distance modulations and not to the Co-Co ones. Indeed, despite the fact the Co-Co distances are nearly constant for the C and D dimers ($\vec{b}$ direction dimers), and strongly fluctuating for the A and B ones ($\vec{a} \pm \vec{b}$ directions dimers)[12], the variation range of both exchanges and hoppings present similar amplitudes (∼7 meV and ∼13 meV respectively). In fact, one should notice that the amplitude of both the super-exchange AFM contribution to J and the hopping integral decrease when the Co-O distance increases.

- J absolute values are very small in amplitude, with average values around 2.56 meV for $\vec{b}$ direction dimers, and -1.54 meV for $\vec{a} \pm \vec{b}$ direction dimers (see Table I). The NN exchange is thus mostly ferromagnetic along the $\vec{b}$ direction and antiferro-

magnetic along the $\vec{a} \pm \vec{b}$ directions.

System	Na_xCoO_2			$Ca_3Co_4O_9$
x	0	0.35	0.5	~ 0.62
J (meV)	-52[13]	-36[20]	-11/-19/-19/-27[13]	[-2.5,10.3] / [-5.0,2.0]

Table II. Effective exchange values (in meV) as a function of the CoO_2 filing parameter x, present system compared to different compounds of the Na_xCoO_2 family.

Comparing these exchange values with the ones obtained in the Na_xCoO_2 family, one sees that while for the superconducting system[20] ($x = 0.35$), the $x = 0.5$ and the $x = 0$ systems[13] the exchange are always AFM, in the present system both AFM and FM interactions were found according to the Co–Co bond. In fact the antiferromagnetic character of J decreases with increasing x (see table II) for the Na_xCoO_2 compounds. These theoretical findings are in agreement with experimental data. Indeed, for low x values the CoO_2 layers of the Na_xCoO_2 systems were found to be antiferromagnetically coupled[16], while for large x values, neutrons scattering exhibit A-type antiferromagnetism[29], that is ferromagnetic correlations within the CoO_2 layers which are anti-ferromagnetically coupled. In fact, Lang *et al* NMR studies[4] allowed to propose a magnetic phases diagram with a temperature dependant boundary between the AFM and FM correlations within the CoO_2 layers. At low temperature the critical doping $x*$ is in the $0.6 \leq x^* \leq 0.7$ range and decreases with increasing temperature ($x^*(300\,\mathrm{K}) \sim 0.5$). Comparing now our computed J values for the $Ca_3Co_4O_9$ compound with both theoretical and experimental results for the Na_xCoO_2 family, one sees that the present compound — associated with $x \sim 0.62$ — compares well with the Na_xCoO_2 family. Indeed, it fluctuating FM/AFM effective exchange agrees well with its assumed doping of the CoO_2 layers close to the phase boundary.

B. Effective on-site repulsion

Figure 5 reports the difference between the average on-site repulsion on a dimer, $\bar{U}$, and the NN repulsion V: $\bar{U} - V = (U_1 + U_2)/2 - V_{12}$. The structural analysis shows us that the Co–Co distance variation is very weak for the $\vec{b}$ direction dimers, while it is large for the $\vec{a} \pm \vec{b}$ dimers (See figure 5). Since the NN repulsion is essentially related to the Co–Co distances one can assume that V is nearly constant along the $\vec{b}$ direction, but strongly varies along the $\vec{a} \pm \vec{b}$ one. Let us analyze figure 5 in this light. The $\bar{U} - V$ curve exhibits only weak modulations for the C dimers. Since both V and U can be assumed as nearly constant for these dimers, the observed modulations may be related to either of them. In any case one can conclude that U remains large and nearly constant from site to site (fluctuations range smaller than 0.2 eV to be compared to an average $\bar{U} - V$ of 3.88 eV). The sites along the A, B and C, D dimers being the same, it results that the strong variation observed on the $\vec{a} \pm \vec{b}$ direction dimers is essentially due to NN repulsion variations $V(\tau)$ associated with the strong fluctuations of the Co–Co distances. The amplitude of the variation is quite large, with about 1eV for an average value of 3.5eV (see table III). It is not possible using our data to quantify further the NN repulsion, however our results suggest that V is large (a few eV in amplitude). An accurate simple model should thus take into account the NN repulsion between the a_{1g} orbitals and its strong variations ; the on-site repulsion being taken as site-independent. The average values $\bar{U} - V$ values found in the present work are consistent with the values found for the Na_xCoO_2 family. Indeed the super-conducting compound exhibits $U - V = 3.6$ eV while it was found for the $Na_{0.5}CoO_2$ system 2.6 eV and 2.8 eV according to the crystallographic site.

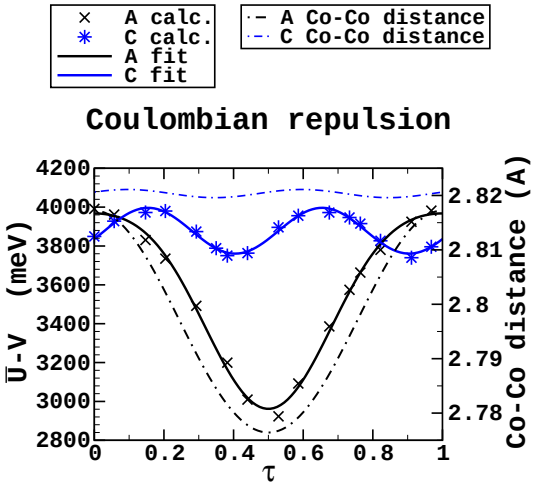

Figure 5. (Color online) Left scale : difference (meV) between the average on-site repulsion on a dimer $\langle U \rangle$ and the effective NN repulsion V as a function of the fourth crystallographic dimension parameter τ. Right scale : Co–Co NN distances (Å) as a function of τ.

Dimer	a_0	a_1	a_2	ζ
A	3542	503	-78	0
C	3878	0	-118	0.1

Table III. Parameters for $\bar{U} - V$ fits according to the equation $\bar{U}(\tau) - V(\tau) = a_0 + a_1 \cos(2\pi[\tau + \zeta]) + a_2 \cos(4\pi[\tau + \zeta])$, where τ is the fourth crystallographic dimension parameter.

C. Effective a_{1g} orbital energy

The on-site repulsion being considered constant, the energy difference between NN a_{1g} orbitals can be extracted from our results. Figure 6 reports the effective

a_{1g} orbital energy : $\varepsilon_{a_{1g}}(\tau)$ ($\varepsilon_{a_{1g}}(0)$ being taken as the energy reference). One can see that the amplitude of the

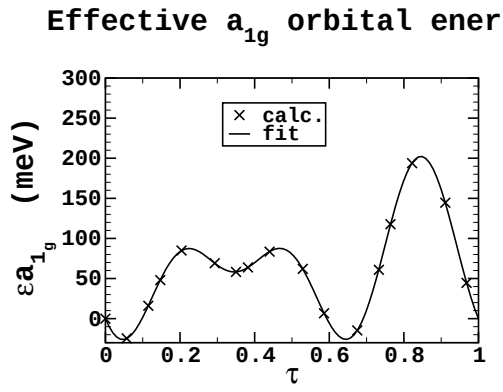

Figure 6. a_{1g} orbital energy (meV) as a function of τ. The $\tau = 0$ value is taken as the energy reference.

$\varepsilon_{a_{1g}}(\tau)$ modulations is quite large ($> 200\,$meV). Compared to this modulation, the a_{1g}–e'_g energy splitting is negligible with an amplitude 10 times weaker. It results that the $\varepsilon_{a_{1g}}(\tau)$ modulation can be seen as an effective potential on the whole cobalt atom. Associated with the strong NN repulsion V[30], one can thus expect a partial charge localization, with Co^{3+} ions on the low energy sites. This result agrees with the observations on the Na_xCoO_2 family for which a partial charge localization is observed for $x \geq 0.5$[31].

V. DISCUSSION

Let us now take a closer look on the Seebeck coefficient in the $Ca_3Co_4O_9$ system. The first point to be stressed is the fact that the TEP can be quite different according to the intercalation layer ($S^{300K}(Na_{0.7}CoO_2) \simeq 100\mu V/K^3$, $S^{300K}([Ca_2CoO_3]_{0.62}[CoO_2]) \simeq 120\mu V/K$[6,10], $S^{300K}([CaBiO_2]_2[CoO_2]_{1.69}) \simeq 160\mu V/K$[32]). The second point is the shape of the Seebeck coefficient as a function of temperature. At low temperature the Seebeck coefficient increases quasi-linearly up to $\sim$100 K and then saturates to a constant value up to about $\sim$400 K[33]. These two behaviors can be fitted on a correlated Fermi liquid behavior, for the low temperature part[34] ($T < 100$ K), and on a Heikes type of configurational entropy for the saturating part[35] ($150\,\text{K} \leq T \leq 400\,\text{K}$).

The generalized Heikes formula[36] is a high temperature approximation. It supposes that the system is at very large temperature compared to the scale of the low energy degrees of freedom. In the present compound we showed (see section III) that these degrees of freedom are associated with the a_{1g} orbital of the CoO_2 layers cobalt atoms 3*d*-shell. Using this formula and the non-degenerated character of the magnetic a_{1g} orbital, one finds (using a cobalt valency of 3.38 as discussed previously in section II), a TEP value of $125\,\mu$V/K. This value is in good agreement with the experimental value of $120\,\mu$V/K found for the $Ca3Co_4O_9$ saturation plateau[6,10]. One may conclude from this agreement that, at room temperature, the high temperature limit of the triangular one band model based on the a_{1g} orbitals is already reached. However, room temperature only corresponds to 25 meV, while the band width of a tight binding model on a triangular lattice is $W = 9|t|$; using our present transfer estimations ($|t| \geq 100\,$meV) it comes a band width of the order of 10000 K. How can we account for such a large difference in order of magnitude? Why does the Heikes model fits so nicely the room temperature Seebeck coefficient for the CoO_2-based compounds?

Different arguments can be advanced in order to explain this high temperature behavior of the TEP at 300 K.

Let us first analyze the behavior of the Seebeck coefficient, as a function of temperature within a one-band tight binding model on a triangular lattice. The Boltzmann equation yields the following Seebeck expression

$$S(T) = -\frac{e}{k_B T}\frac{\int(\varepsilon-\mu)\frac{\partial f_0}{\partial \varepsilon}d\varepsilon}{\int \frac{\partial f_0}{\partial \varepsilon}d\varepsilon} \tag{4}$$

$$= -\frac{e}{k_B T}\frac{\int \varepsilon\frac{\partial f_0}{\partial \varepsilon}d\varepsilon}{\int \frac{\partial f_0}{\partial \varepsilon}d\varepsilon} + \frac{e}{k_B T}\mu \tag{5}$$

$$= S_{tr}(T) + S_\mu(T) \tag{6}$$

$$\tag{7}$$

where $f_0(T,\varepsilon)$ is the Fermi function, ε the orbitals energy, μ the electrochemical potential ; the collision time as well as the degeneracy is supposed energy independent. Figure 7 reports $S(T)$ and its two components $S_{tr}(T)$ and $S_\mu(T)$. At low temperature $S_{tr}(T)$ dominates, reaches a maximum for $T/W \sim 1/4$, then slowly decreases toward zero in the high temperature limit. On the contrary the entropic part $S_\mu(T)$ increases for all temperatures and reaches its high temperature limit for temperatures of the order of a few band widths. The sum of the two terms results in a Seebeck coefficient reaching its saturation value at much lower temperature than its entropic part. Indeed for $T/W = 0.5$, S is already larger than 90% of its high temperature value. This simple analysis already allows us to reduce, from a few band widths to half the band width, the estimation of the temperature at which the TEP saturation should be observed. This is however not enough to account for the observed saturation temperature. Indeed $W/2 = 9|t|/2$ still accounts for about 5000 K.

A second argument is the extremely large value of the correlation strength in these compounds. Indeed, our calculations yield for the average U/t a value of 26. Despite this very large U/t, transport measurements[6,10] find the system metallic. One thus expect its Fermi level quasiparticle pic to be strongly renormalized due to the strong correlation effects[37].

Finally let us remember that our results suggest a partial electron localization due the large site energy mod-

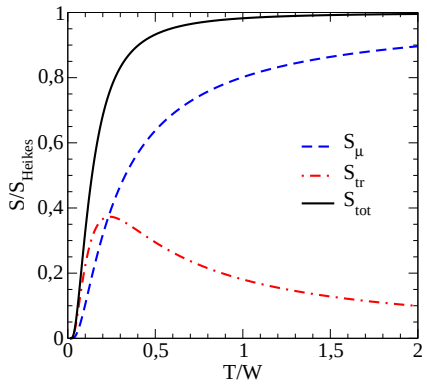

Figure 7. (Color online) Seebeck coefficient of a triangular lattice as a function of the temperature, normalized to the band width. Blue dashed curve : the entropic term : $S_\mu(T)$, red dot-dashed curve : the Fermi liquid part : $S_{tr}(T)$.

ulation ($> 200\,\mathrm{meV}$) and a large value of NN repulsion. It results that the lattice pattern seen by the Fermi level electrons can be expected to be quite different from the homogeneous triangular lattice assumed in these systems. This effect is also expected to strongly reduce the quasi-particle bandwidth at the Fermi level.
All together, it seems quite possible that the bandwidth reduction is large enough (20 to 30 times) so that $0.5W_{\mathrm{eff}} \sim 200\,\mathrm{K}$, and thus that the high temperature Heikes model appears valid for the present (and related) systems.

Let us now take a look on the TEP behavior at temperatures larger than 400 K. Indeed, at $T_c = 396\,\mathrm{K}$ the $Ca_3Co_4O_9$ compound experiences a first-order metal-semiconductor phase transition associated with a linear increase of the Seebeck coefficient for $T > T_c$[33]. Different hypotheses have been proposed in order to account for this phase transition and the high temperature phase properties. The first one associates the transition with a cobalt spin-state transition[10]. However our calculations show that the first atomic excited spin state of the cobalt atom is at least at 700 meV, i.e. 8100 K, above the ground state. Such an energy difference is clearly incompatible with a phase transition energy scale of 400 K. The second hypothesis associates the transition with a change in the cobalt t_{2g} orbitals occupancies. However this hypothesis does not resist to the energy scale of the a_{1g}–e'_g energy splitting found in section III. Indeed, the 240 meV≃2800 K is still far too large for the 400 K energy scale of the transition. The last hypothesis is an electron localization of the e'_g orbitals, associated with a structural phase transition[33]. Even if the assumption that the e'_g orbitals are the Fermi level ones has been proven incorrect (see reference 13 or for the present system section III), the idea of an electron localization induced by an increase of the in-plane distances in the CoO_2 layers seem quite possible and would explain the metal-semi-conductor phase transition. Muguera and Grebille[38] solved the crystallographic structure in the high temperature phase. They showed that the transition is due to a rearrangement of the central CoO layer of the Ca_2CoO_3 subsystem. This rearrangement acts on the CoO_2 layers through the O–Ca interaction between the two subsystems. It results in a modification of both the cobalts and oxygens modulations (but not of the average structure) along the $\vec{a}$ and $\vec{c}$ directions. While such a weak structural modification can account for the metal-semiconductor transition (due to the large correlation strength and associated closeness to the Mott transition), it cannot account for the associated increase of the Seebeck coefficient. Indeed, such an increase necessitate the opening of new degrees of freedom at the Fermi level and the weakness of the structural modifications within the CoO_2 layers cannot account the opening of either the higher cobalt spin states or the e'_g orbitals. This study however show us that there is another degree of freedom up to now ignored that should be taken into account, that is the partial charge localization due to the action of the subsystem modulation over the Fermi level orbital energies. Indeed a modification of the modulation vector will be expected to modify the energy profile pictured in figure 6, thus the charge localization configuration and the lattice pattern seen by the Fermi electrons at the given temperature. Out of any other energetically compatible hypothesis, the latter seems the most plausible.

VI. CONCLUSION

We performed ab initio calculations of the effective local parameters of the thermoelectric $Ca_3Co_4O_9$ compound, taking into account the incommensurate distortions. As in the Na_xCoO_2 family, cobalts a_{1g}–e'_g orbitals splitting is large so that the low energy physics can be accounted for using the a_{1g} orbitals only. We showed that the incommensurate modulation of the CoO_2 layer cannot be neglected in order to understand the compound physical properties. Indeed, site energies, NN exchange, NN hopping as well as first neighbor repulsions are strongly modulated due to the misfit character of the system. It particular the site energies large modulation let us expect a partial Fermi electrons localization. The effective exchange remains weak in amplitude, however fluctuates between antiferromagnetic coupling and ferromagnetic one. This results can be compared with the on-plane AFM-FM transition line in the Na_xCoO_2 family associated at $T = 0\,\mathrm{K}$ with similar cobalt valency as found in the present compound.

We discussed the temperature behavior of the Seebeck coefficient and showed that the cobalts a_{1g} orbitals bandwidth is strongly renormalized, due to very strong electron correlation ($U/t \sim 26$), and the modification of the effective lattice pattern seen by the itinerant electrons, associated with the partial charge localization. This strong bandwidth renormalization is most proba-

bly responsible for the plateau due to the high temperature behavior observed in the Seebeck coefficient on the [150 K, 400 K] range. We further showed that he sudden increase of the TEP for $T > T_c = 396\,\mathrm{K}$, cannot be attributed either by a cobalt spin state change or by a modification of the a_{1g} vs e'_g orbitals occupation. In fact the 396 K metal-semiconductor transition is associated with a structural rearrangement within the Ca_2CoO_3 subsystem inducing a modulation modification within the CoO_2 layer. This modification induces a site energy pattern change and thus a localization pattern change thought to be the best candidate for the change in the Seebeck behavior.

ACKNOWLEDGMENTS

The authors thank Prof. Dominique Grebille and Dr. Olivier Perez for helpful discussion on the crystallographic aspects, as well as Dr. Daniel Maynau for providing us with the CASDI suite of programs. These calculations where done using the CNRS IDRIS computational facilities under project n°1842 and the CRIHAN computational facilities under project n°2007013.

[1] J.-J. Braconnier, C. Delmas, C. Fouassier and P. Hagenmuller, Mater. Res. Bull. **15**, 1797 (1980).
[2] K. Takada, H. Sakurai, E. Takayama-Muromachi, F. Izumi, R. A. Dilanian and T. Sasali, Nature **422**, 53 (2003).
[3] I. Terasaki, Y. Sasago and K. Uchinokura, Phys. Rev. **B 56**, R12685 (1997).
[4] G. Lang, J. Bobroff, H. Alloul, G. Collin and N. Blanchard, Phys. Rev. **B 78**, 155116 (2008).
[5] K. Takahata, Y.Iguchi, T. Itoh, D. Tanaka and I. Terasaaki, Meet. Abstr. (sect Meet 1999), Phys. Soc. Japan, 27 pG-2.
[6] Y. Miyazaki, K. Kudo, M. Akoshima, Y. Ono, Y. Koike and T. Kajitani, Jpn. J. Appl. Phys. **39**, L531 (2000).
[7] Ph. Boullay, B. Domenges, M. Hervieu, D. Groult and B. Raveau, Chem. Mater. **8**, 1482 (1996) ; Ph. Boullay, R. Seshadri, F. Studer, M. Hervieu, D. Groult and B. Raveau, Chem. Mater. **10**, 92 (1998).
[8] M. Hervieu, Ph. Boullay, C. Michel, A. Maignan and B. Raveau, J. Solid State Chem. **142**, 305 (1999).
[9] H. Yamauchi, K. Sakai, T. Nagai, Y. Matsui and M. Karppinen, Chem. Mater. **18** 155 (2006).
[10] A. C Masset, C. Michel, A. Maignan, M. Hervieu, O. Toulemonde, F. Studer, B. Raveau and J. Hejtmanek, Phys. Rev. **B 62**, 166 (2000).
[11] J. Sugiyama, H. Itahara, T. Tani, J. H. Brewer, E. J. Ansaldo, Phys. Rev. **B 66**, 134413 (2002).
[12] H. Muguerra, D. Grebille and F. Bourée, Acta Cryst. **B 64**, 144 (2008).
[13] S. Landron, J. Soret and MB Lepetit, J. Phys. Condens. Matter **22**, 345603 (2010).
[14] R. Asahi, J. Sugiyama and T. Tani, Phys. Rev. **B 66**, 155103 (2002).
[15] D. J Singh, Phys. Rev. **B 68**, R020503 (2003).
[16] T. Fujumoto, G.-Q. Zheng, Y. Kitaoka, R. L. Meng, J. Cmaidalka and C. W. Chu, Phys. Rev. Letters **92**, 047004 (2004) ; J. Bobroff, G. Lang, H. Alloul, N. Blanchard and G. Collin, Phys. Rev. Letters **96**, 107201 (2006) ; C. de Vaulx, M.-H. Julien, C. Berthier, S. Hébert, V. Pralong and A. Maignan, Phys. Rev. Letters **98**, 246402 (2007).
[17] P. Zhang, W. Luo, M. L. Cohen and S. G. Louie, Phys. Rev. Letters **93**, 236402 (2004).
[18] J. Miralles, J. P. Daudey and R. Caballol, Chem. Phys. Letters **198**, 555 (1992) ; M.-B. Lepetit, *Recent Research Developments in Quantum Chemistry 3*, p. 143, Transword Research Network (2002).
[19] See for instance : D. Muñoz, F. Illas and I. de P.R. Moreira, Phys. Rev. Letters **84**, 1579 (2000) ; N. Suaud and MB Lepetit, Phys. Rev. Letters **88**, 056405 (2002) ; S. Petit and M.-B. Lepetit, EPL **87** 67005 (2009).
[20] S. Landron and M.-B. Lepetit, Phys. Rev. **B 74** 184507 (2006).
[21] A. Gellé and M.-B. Lepetit, Phys. Rev. Letters **92**, 236402 (2004) ; Eur. Phys. J. **B 43**, 29 (2005).
[22] N. W. Winter, R. M. Pitzer and D. K. Temple, J. Chem. Phys. **86**, 3549 (1987).
[23] A. Gellé and M.-B. Lepetit, J. Chem. Phys. **128**, 244716 (2008).
[24] Q. Huang, M. L. Foo, R. A. Pascal, Jr., J. W. Lynn, B. H. Toby, Tao He, H. W. Zandbergen, and R. J. Cava, Phys. Rev. **B 70**, 184110 (2004).
[25] G. Yang, R. F. Klie and Q. Ramasse, Phys. Rev. **B 78**, 153109 (2008).
[26] Z.Barandiaran and L.Seijo, Can. J. Chem. **70**, 409 (1992).
[27] Y. Miyazaki, M. Onoda, T. Oku, M. Kikuchi, Y. Ishii, Y. Ono, Y. Morii and T. Kajitani, J. Phys. Soc. Japan **71**, 491 (2002).
[28] S. Landron and M.-B. Lepetit, Phys. Rev. **B 77**, 125106 (2008).
[29] A. T. Boothroyd, R. Coldea, D. A. Tennant, D. Prabhakaran, L. M. Helme and C. D. Frost, Phys. Rev. Letters **92**, 197201 (2004) ; S. P. Bayrakci, I. Mirebeau, P. Bourges, Y. Sidis, M. Enderle, J. Mesot, D. P. Chen, C. T. Lin and B. Keimer, Phys. Rev. Letters **94**, 157205 (2005).
[30] T. Watanabe, H. Yokoyama, Y. Tanaka, J-I. Inoue, J. Phys. Chem. Solids **69**, 3372 (2008).
[31] G. Lang, J. Bobroff, H. Alloul, I. Mukhamedshina, G. Collin and N. Blanchard, J. Alloys Comp. **480**, 144 (2009) ; H. Alloul, I. R. Mukhamedshin, T. A. Platova and A. V. Dooglav, EPL **85**, 47006 (2009).
[32] E. Guilmeau, M. Pollet, D. Grebille, M. Hervieu, H. Muguerra, R. Cloots, M. Mikami and R. Funahashi, Inorg. Chem. **46**, 2124 (2007).
[33] J. Cheng, Y. Sui, Y. Wang, X. Wang, W. Su, Appl. Phys. **A 94**, 911 (2009).
[34] P. Limelette, V. Hardy, P. Auban-Senzier, D. Jérome, D. Flahaut, S. Hébert, R. Frésard, Ch. Simon, J. Noudem and A. Maignan, Phys. Rev. **B 71**, 233108 (2005).
[35] M. Pollet, J.-P. Doumerc, E. Guilmeau, D. Grebille, J.F. Fagnard and R. Cloots, J. Appl. Phys. **101**, 83708 (2007).
[36] J.-P. Doumerc, J. Solid State Chem. **110**, 419 (1994).

[37] X. Y. Zhang, M. Rozenberg, and G. Kotliar, Phys. Rev. Letters **70**, 1666 (1993).
[38] H. Muguerra and D. Grebille, Acta Cryst. **B 64**, 676 (2008).